Structural symmetry and magnetocrystalline anisotropy of $SrRuO_3$ films on $SrTiO_3$

M. Ziese*
Division of Superconductivity and Magnetism, University of Leipzig, D-04103 Leipzig, Germany

I. Vrejoiu† and D. Hesse
Max Planck Institute of Microstructure Physics, D-06120 Halle, Germany

(Received 23 November 2009; revised manuscript received 23 February 2010; published 18 May 2010)

The structural, magnetic, and magnetotransport properties of $SrRuO_3$ films grown on $SrTiO_3$ (001) substrates were investigated with the aim to determine the crystalline symmetry, crystalline orientation, and magnetocrystalline anisotropy of an ultrathin (5 nm) $SrRuO_3$ film. 60- and 40-nm-thick $SrRuO_3$ films were extensively studied by transmission electron microscopy as well as magnetic and magnetotransport techniques, respectively. These studies showed orthorhombic symmetry with a slight monoclinic distortion and a well-defined long-range order of crystallographic domains with the $[001]_o$ axis parallel to terraces on the slightly vicinal $SrTiO_3$ substrate. The magnetocrystalline anisotropy is very strong. The easy axis lies in the $(001)_o$ plane under a temperature-dependent angle of about 35° with respect to the $[110]_o$ direction that is along the film normal. Below 70 K indications for a spin reorientation transition were detected. The angular-dependent anisotropic magnetoresistance shows distinctive characteristics of the monoclinic symmetry that can be used as a fingerprint. Transmission electron microscopy images of the 5 nm thin $SrRuO_3$ film show a coherently strained state. Using the fingerprints from the angular magnetoresistance it could be clearly shown that this ultrathin $SrRuO_3$ film, although grown in step flow growth as well, has still monoclinic symmetry, but lacks long-range order of the crystallographic domains. A fraction of 30–40 % of misaligned domains (rotated in plane by 90°) was estimated from the magnetoresistance curves.

DOI: 10.1103/PhysRevB.81.184418 PACS number(s): 75.70.Ak, 75.60.−d, 75.47.Lx

I. INTRODUCTION

$SrRuO_3$ (SRO) is one of the few itinerant oxide ferromagnets. Bulk SRO crystallizes in an orthorhombic phase,[1] has a Curie temperature of about 160 K and a magnetic moment per Ru ion of about $1.6\mu_B$/Ru.[2] SRO films grow on $SrTiO_3$ (001) substrates with the orthorhombic $[110]_o$ direction along the surface normal; within the substrate plane crystallographic domains with $[001]_o$ and $[1\bar{1}0]_o$ orientation along one of the cubic $SrTiO_3$ directions might form. Long-range ordering of these crystallographic domains can be achieved by growth on vicinal $SrTiO_3$ substrates with well developed, unit-cell high terraces, since the $[001]_o$ direction aligns along the terrace edge direction.

The structural symmetry and magnetocrystalline anisotropy of SRO films grown on $SrTiO_3$ were studied in a series of papers.[3–9] The films under study, however, were comparatively thick to ensure a sufficient signal-to-noise ratio for the various structural and magnetic techniques. However, recently strong antiferromagnetic interlayer exchange coupling was found in SRO/LSMO superlattices with very thin SRO layers in the range 3–8 nm.[10] Here LSMO stands for the double exchange ferromagnet $La_{0.7}Sr_{0.3}MnO_3$. Magnetization direction and exchange-bias field in these superlattices sensitively depend on the individual thickness of the SRO layers through the strong magnetocrystalline anisotropy of SRO. Since reliable data for the structural symmetry and magnetocrystalline anisotropy of such thin films were not available in the literature, we decided to study these properties with a variety of techniques. In this work the structural, magnetic, and magnetotransport properties of SRO single-layer films were investigated with a specific focus on the development of magnetoresistance measurements as a sensitive probe for the crystalline symmetry and magnetocrystalline anisotropy. In Sec. II the angular dependence of the magnetocrystalline anisotropy energy and magnetoresistance are derived, in Sec. III the experimental procedure is outlined; Sec. IV presents main results and conclusions; the paper is concluded with a brief summary in Sec. V.

II. THEORETICAL CONSIDERATIONS

In general both anisotropy energy and resistivity are functions of the magnetization direction. The functional dependence is *a priori* unknown but is restricted by the crystalline symmetry. It is standard procedure to expand the anisotropy energy or resistivity in powers of the direction cosines of the magnetization vector and to restrict the number of expansion coefficients by group theoretical methods. For this one might follow the procedure outlined by Birss[11] which was done for Mn-doped GaAs films in Refs. 12 and 13; or one can follow the work of Döring and Simon,[15,16] who derived the dependence of the magnetocrystalline energy[14] and the magnetoresistance on the direction of the magnetization for all crystal systems in closed form. Here the second route is followed.

The magnetoresistance $\Delta\rho/\rho_0$ can be written as a function of a symmetric tensor of second rank $(A_{ij})_{i,j=1,3}$ reduced by the unit vector $(\beta_1,\beta_2,\beta_3)$ of the current density,

$$\Delta\rho/\rho_0 = \sum_{i,j=1}^{3} A_{ij}\beta_i\beta_j. \quad (1)$$

By definition the β_i are the direction cosines of the current density with respect to the crystallographic basis vectors.

The tensor components A_{ij} are functions of the direction cosines of the magnetization, $\vec{M}=M_S\hat{m}=M_S(\alpha_1,\alpha_2,\alpha_3)$, where M_S denotes the saturation magnetization and $\hat{m}$ the unit vector along the magnetization direction. The functional form of the matrices $(A_{ij})_{i,j=1,3}$ was obtained from crystal symmetry considerations in Refs. 14–16. Note that in case of crystal systems with a normal basis, the direction cosines obey $\alpha_1^2+\alpha_2^2+\alpha_3^2=\beta_1^2+\beta_2^2+\beta_3^2=1$.

Since the crystalline symmetry of SRO films on $SrTiO_3$ (001) is under debate, one has to consider various options for the symmetry. Bulk $SrRuO_3$ is orthorhombic with symmetry group *Pbnm* and lattice constants at room temperature of $a=0.55670$ nm, $b=0.55304$ nm, and $c=0.78446$ nm.[1] In the standard view SRO grows on cubic $SrTiO_3$ with the $[110]_o$ direction along the surface normal and the $[001]_o$ direction along a $SrTiO_3$ in-plane basis vector.[3] Long-range directional order in the $[001]_o$ direction is induced by the presence of terraces in vicinal substrates; the $[001]_o$ direction is along the unit-cell height steps of these terraces. It was reported, however, that in SRO films the orthorhombic structure is distorted to a triclinic structure[3] with small angular deviations on the order of 1°.[3] On the other hand, since strain effects are known to be important,[17,18] one might argue that very thin SRO films grown on $SrTiO_3$ are fully strained such that a tetragonal structure is induced in the films.[8,19] This tetragonal cell might consist either of a single perovskite cell with $a=b=a_{SrTiO_3}$ (Ref. 19) or of four perovskite cells with the $[100]_t$ and $[010]_t$ directions aligned with the face diagonals of the cubic $SrTiO_3$ cell.[8] The subscripts *t*, *o*, and *m* used in the text refer to indexing in the tetragonal, orthorhombic, and monoclinic system. The directions in the figures are specified by the standard orthorhombic cell without using subscripts.

In the following the expressions for the anisotropy energy density and the anisotropic magnetoresistance resistivity are derived for the tetragonal, orthorhombic, and monoclinic structure. The monoclinic structure was chosen here instead of the triclinic structure to minimize the number of expansion coefficients. Figure 1 shows a sketch of an orthorhombic crystal system with the magnetization unit vector indicated. The unit vector of the magnetization is written in the laboratory system (*xyz* system) as $\hat{m}=(\sin\theta\cos\varphi,\sin\theta\sin\varphi,\cos\theta)$ with standard definitions of the angles θ and φ with respect to the *z* and *x* axes. The direction cosines of the magnetization $(\alpha_1,\alpha_2,\alpha_3)$ are defined with respect to the crystallographic axes of the SRO film. Therefore the SRO film has to be oriented with respect to the laboratory system and the direction cosines are then found by projection of $\hat{m}$ onto the respective crystallographic axes. In case of the orthorhombic and monoclinic symmetry the orientation of the SRO film with respect to the laboratory system was chosen as indicated in the figure, i.e., the surface normal $[110]_{o,m}$ was along the *z* axis and the in-plane $[001]_{o,m}$ direction along the *x* axis. Experimentally the magnetization vector was rotated either in the $(1\bar{1}0)_o$ plane ($\varphi=0°$ and varying θ) or in the $(001)_o$ plane ($\varphi=90°$ and varying θ). The angle between the $[100]_o$ direction and the substrate surface is taken to be exactly 45° since the deviations will be smaller than our absolute angular resolution. By the same argument, in the monoclinic structure, the angular deviation from 90° between the $[100]_m$ and $[010]_m$ axes is neglected, i.e., use is only made of the more general functional forms of the orthorhombic and monoclinic symmetries, but not of the small angular deviations. In case of the tetragonal structure, two orientations are possible: whereas the $[001]_t$ axis is always parallel to the *z* axis, along the *x* axis either the $[100]_t$ or $[110]_t$ axis might be oriented as discussed above. Here only the first case is treated, the second leads to the same form of the expansion.

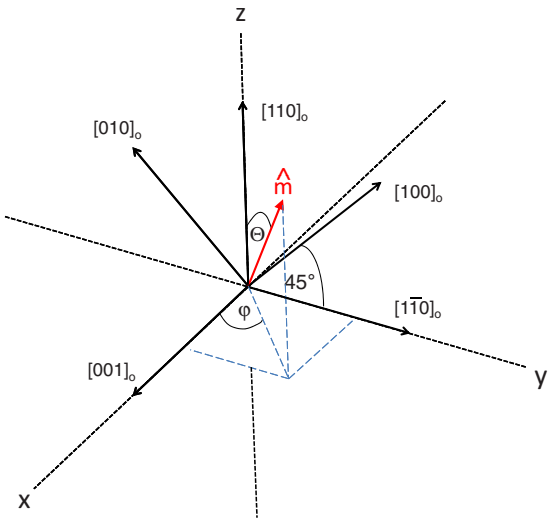

FIG. 1. (Color online) Sketch of the magnetization unit vector $\hat{m}$ in the laboratory frame (*xyz* frame) with the definition of the angles θ and φ indicated. Further the orientation of the SRO film with respect to the laboratory system is shown using indexing in the orthorhombic system.

A. Tetragonal symmetry (D_{4h})

In this case magnetization rotations in the $(100)_t$ and $(010)_t$ planes are equivalent with $\alpha_1=\sin\theta$, $\alpha_2=0$, and $\alpha_3=\cos\theta$. In the longitudinal current direction $\beta_1=1$, $\beta_2=\beta_3=0$ and in the transverse current direction $\beta_1=\beta_3=0$ and $\beta_2=1$. Therefore one only has to consider the tensor components A_{11} and A_{22}. From Ref. 15 one obtains $A_{11}=B(\alpha_1^2,\alpha_3^2)$ and $A_{22}=B(\alpha_2^2,\alpha_3^2)$ with an unknown analytic function *B*. Expanding *B* in the α_i's and rearranging yields for the longitudinal case,

$$\Delta\rho/\rho_0=c_0+\sum_{n=1}^{\infty}c_{2n}\cos(2n\theta) \tag{2}$$

and for the transverse case

$$\Delta\rho/\rho_0=c_0'+\sum_{n=1}^{\infty}c_{2n}'\cos(2n\theta) \tag{3}$$

with expansion coefficients c_{2n} and c_{2n}'.

The anisotropy energy density is given by $E_K=F(s,p)$ with $s=\alpha_3^2$, $p=\alpha_1^2\alpha_2^2$ and the analytic function $F(s,p)$.[14] For a magnetization rotation in the $(010)_t$ plane one obtains

$$E_K = K_0 + \sum_{n=1}^{\infty} K_{2n} \cos(2n\theta). \quad (4)$$

B. Orthorhombic symmetry (D_{2h})

In orthorhombic symmetry one has two main nonequivalent rotation planes, namely, the $(001)_o$ and $(1\bar{1}0)_o$ planes; considering the longitudinal and transverse configuration in total four cases have to be discussed.

1. Rotation plane: $(001)_o$*, current along* $[1\bar{1}0]_o$

The direction cosines are given by $\alpha_1 = (\sin\theta + \cos\theta)/\sqrt{2}$, $\alpha_2 = (-\sin\theta + \cos\theta)/\sqrt{2}$, and $\alpha_3 = 0$. The direction cosines of the current density are $\beta_1 = 1/\sqrt{2}$, $\beta_2 = -1/\sqrt{2}$, and $\beta_3 = 0$. Then

$$\Delta\rho/\rho_0 = \beta_1^2 A_{11} + \beta_2^2 A_{22} + \beta_1\beta_2 A_{12}. \quad (5)$$

Expansion in the α_i's and rearranging yields

$$\Delta\rho/\rho_0 = c_0 + \sum_{n=1}^{\infty} s_{2n} \sin(2n\theta) + \sum_{n=1}^{\infty} c_{2n} \cos(2n\theta). \quad (6)$$

2. Rotation plane: $(001)_o$*, current along* $[001]_o$

In this case $\beta_1 = \beta_2 = 0$ and $\beta_3 = 1$ finally yielding

$$\Delta\rho/\rho_0 = c_0' + \sum_{n=1}^{\infty} s_{4n-2} \sin[(4n-2)\theta] + \sum_{n=1}^{\infty} c_{4n}' \cos(4n\theta). \quad (7)$$

3. Rotation plane: $(1\bar{1}0)_o$*, current along* $[001]_o$

The direction cosines are $\alpha_1 = \alpha_2 = \cos\theta/\sqrt{2}$ and $\alpha_3 = \sin\theta$; with $\beta_1 = \beta_2 = 0$ and $\beta_3 = 1$ one finds

$$\Delta\rho/\rho_0 = c_0'' + \sum_{n=1}^{\infty} c_{2n}'' \cos(2n\theta). \quad (8)$$

4. Rotation plane: $(1\bar{1}0)_o$*, current along* $[1\bar{1}0]_o$

The direction cosines of the current density are $\beta_1 = 1/\sqrt{2}$, $\beta_2 = -1/\sqrt{2}$, and $\beta_3 = 0$; the symmetry is the same as in the previous case,

$$\Delta\rho/\rho_0 = c_0''' + \sum_{n=1}^{\infty} c_{2n}''' \cos(2n\theta). \quad (9)$$

5. Anisotropy energy density

The anisotropy energy density is given by $E_K = F(s,p)$ with $s = \alpha_1^2$, $p = \alpha_2^2$ and the analytic function $F(s,p)$.[14] For a magnetization rotation in the $(001)_o$ plane one obtains

$$E_K = K_0 + \sum_{n=1}^{\infty} K_{4n-2} \sin[(4n-2)\theta] + \sum_{n=1}^{\infty} K_{4n} \cos(4n\theta), \quad (10)$$

whereas a magnetization rotation in the $(1\bar{1}0)_o$ plane leads to

$$E_K = K_0' + \sum_{n=1}^{\infty} K_{2n}' \cos(2n\theta). \quad (11)$$

C. Monoclinic symmetry (C_{2h})

Since the orientation of the monoclinic cell with respect to the $SrTiO_3$ substrate is the same as that of the orthorhombic cell, the discussion is analogous to the orthorhombic case.

1. Rotation plane: $(001)_m$*, current along* $[1\bar{1}0]_m$

In this case the same result as for the orthorhombic symmetry is obtained. This is intuitively clear since Eq. (6) already had the most general form for the expansion such that further symmetry lowering does not have any effect on this expression,

$$\Delta\rho/\rho_0 = c_0 + \sum_{n=1}^{\infty} s_{2n} \sin(2n\theta) + \sum_{n=1}^{\infty} c_{2n} \cos(2n\theta). \quad (12)$$

2. Rotation plane: $(001)_m$*, current along* $[001]_m$

In this case the expansion is changed compared to the orthorhombic case,

$$\Delta\rho/\rho_0 = c_0' + \sum_{n=1}^{\infty} s_{2n}' \sin(2n\theta) + \sum_{n=1}^{\infty} c_{2n}' \cos(2n\theta). \quad (13)$$

3. Rotation plane: $(1\bar{1}0)_o$*, current along* $[001]_o$

$$\Delta\rho/\rho_0 = c_0'' + \sum_{n=1}^{\infty} c_{2n}'' \cos(2n\theta). \quad (14)$$

4. Rotation axis: $(1\bar{1}0)_o$*, current along* $[1\bar{1}0]_o$

$$\Delta\rho/\rho_0 = c_0''' + \sum_{n=1}^{\infty} c_{2n}''' \cos(2n\theta). \quad (15)$$

5. Anisotropy energy density

The anisotropy energy density is given by $E_K = F(s,p) + qG(s,p)$ with $s = \alpha_1^2$, $p = \alpha_2^2$, $q = \alpha_1\alpha_2$, and the analytic functions $F(s,p)$ and $G(s,p)$.[14] For a magnetization rotation in the $(001)_o$ plane one obtains

$$E_K = K_0 + \sum_{n=1}^{\infty} K_{s2n} \sin(2n\theta) + \sum_{n=1}^{\infty} K_{c2n} \cos(2n\theta), \quad (16)$$

whereas a magnetization rotation in the $(1\bar{1}0)_o$ plane leads to

$$E_K = K_0' + \sum_{n=1}^{\infty} K_{2n}' \cos(2n\theta). \quad (17)$$

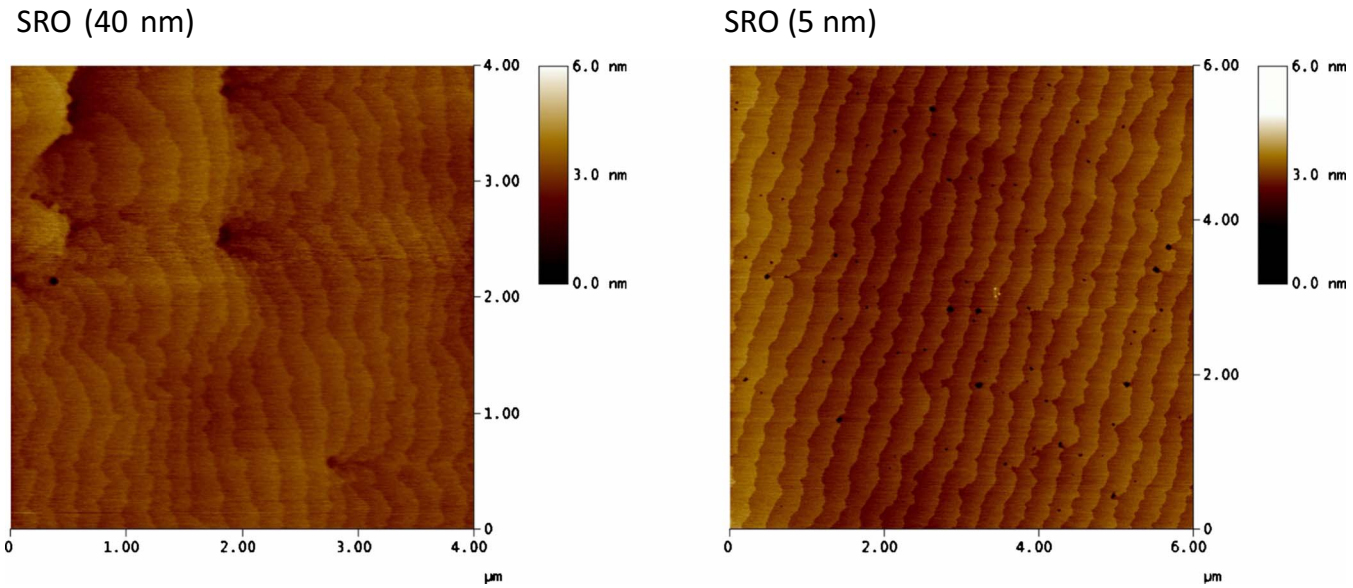

FIG. 2. (Color online) AFM topography image of the (a) 40-nm-thick and (b) 5-nm-thick $SrRuO_3$ films.

III. EXPERIMENTAL

The $SrRuO_3$ films were fabricated by pulsed laser deposition (KrF laser, 248 nm) from a stoichiometric polycrystalline target. Vicinal $SrTiO_3$ (100) substrates with small miscut angle were employed for the deposition, after being etched and annealed to have atomically flat top surfaces with uniform TiO_2 termination and terrace morphology (typically 150–400 nm terrace width). Substrate temperature and oxygen partial pressure were 650 °C and 0.14 mbar O_2, respectively. In this study three films with thickness of 5, 40, and 60 nm were investigated. The 60-nm-thick film was used for extensive transmission electron microscopy (TEM) measurements, the other films were used for magnetization and magnetotransport measurements. Curie temperatures were about 143 K in case of the 5 nm and 145 K in case of the 40-nm-thick film.

The films were characterized by atomic force microscopy (AFM) and TEM. AFM topography images were recorded by help of an atomic force microscope of type CP Research (Veeco). From the 60-nm-thick SRO film, both a plan-view and a cross-section sample for TEM were prepared by successively cutting, gluing, mechanical polishing, dimpling, and ion beam thinning the sample; from the film of 5 nm thickness, a plan-view sample was prepared. TEM and selected area diffraction (SAED) investigations were carried out in a transmission electron microscope of type CM20T (Philips) working with a primary electron energy of 200 keV.

The resistance and magnetoresistance were measured by a standard four-point configuration. The films were mounted on a rotatable sample holder in a helium flow cryostat (Oxford Instruments) equipped with a superconducting solenoid with maximum fields of 9 T. The rotation axis was perpendicular (precision of ±1°) to the vertical magnetic field. Angular sweeps of the magnetoresistance were made in the angle range $-45° \leq \theta_F \leq 135°$, where θ_F denotes the angle between the magnetic field and the surface normal of the film. The angular position of the film was aligned before insertion into the cryostat; angular accuracy was ±3° for alignment of the sample edges as well as alignment between surface normal and magnetic field direction. Angular hysteresis after reversal of the sweep direction was below ±0.1°.

Field- and temperature-dependent magnetization measurements were performed in a MPMS-7 or MPMS-XL superconducting quantum interference device (SQUID) magnetometer (Quantum Design) with the samples mounted in a straw. The angular alignment in these measurements is not better than ±5°. After finishing the resistance measurements the 40-nm-thick SRO sample was broken into various pieces. Angular-dependent magnetization measurements were made on two of these pieces using the horizontal rotator of the MPMS-XL SQUID magnetometer. The angular accuracy of this setup is ±3° with respect to the surface normal and it has an angular hysteresis of ±3° after reversal of the sweep direction.

IV. RESULTS AND DISCUSSION

A. Structural characterization

Figure 2 shows AFM images of 4×4 μm^2 and 6×6 μm^2 regions of the 40-nm-thick and 5-nm-thick SRO films, respectively. In both cases clear terraces of unit-cell height could be seen (step-flow growth regime) similar to the results on the growth of $PbZr_{0.2}Ti_{0.8}O_3$ (Ref. 20) and $La_{0.7}Sr_{0.3}MnO_3$ (Ref. 21) films. Terrace widths were about 200 nm and 300 nm, respectively, yielding a miscut angle of about 0.1°.

Figure 3 shows a plan-view TEM image, as well as the related SAED pattern as inset. The latter is properly oriented with respect to the TEM image. A magnified (and rotated) view of part of this diffraction pattern is shown in Fig. 4, however now indexed according to a simulation and a corresponding comparison with literature.[22,23] From this indexing, the zone axis is obtained as $[001]_o \times [1\bar{1}0]_o = [110]_o$, which allows to deduce the film normal $[110]_o$. The correspond-

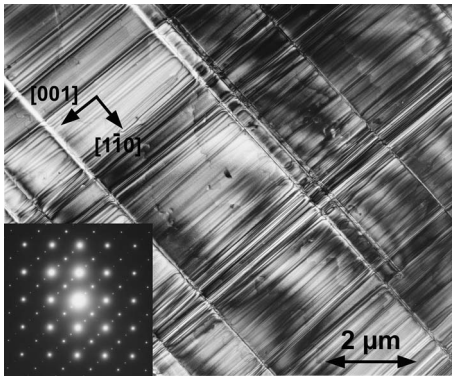

FIG. 3. Plan-view TEM image of the 60-nm-thick $SrRuO_3$ film with crystallographic directions indicated. The inset shows the related selected area diffraction pattern, which is properly oriented with respect to the TEM image.

ingly deduced azimuthal crystallographic directions are indicated in the image of Fig. 3. It appears that a coarse mesh of misfit dislocations at the $SrRuO_3/SrTiO_3$ interface is visible, running along $[001]_o$ and $[1\bar{1}0]_o$ directions, with dislocation distances on the order of 500 nm to 3 μm.[24] The narrow-spaced lines along the $[001]_o$ direction are most probably bending contours related to the steps of the vicinal substrate. (Note that the entire sample is very thin, allowing for bending.) According to the miscut of about 0.1°, the steps of the step-terrace structure on the $SrTiO_3$ surface have a spacing of about 200–300 nm, which well corresponds to the order of magnitude of the line distance in the figure. The fact that the SRO $[1\bar{1}0]_o$ direction is perpendicular to the steps of the vicinal $SrTiO_3$ substrate exactly corresponds to previous findings, see Ref. 3.

Figure 5 is a cross-section TEM image of the same film, together with the corresponding diffraction pattern shown in the inset. Again, the crystallographic directions deduced from the diffraction pattern are inserted. The thickness of the smooth and plane film is 60 nm. No steps are visible at the $SrRuO_3/SrTiO_3$ interface, because the sample has been cut

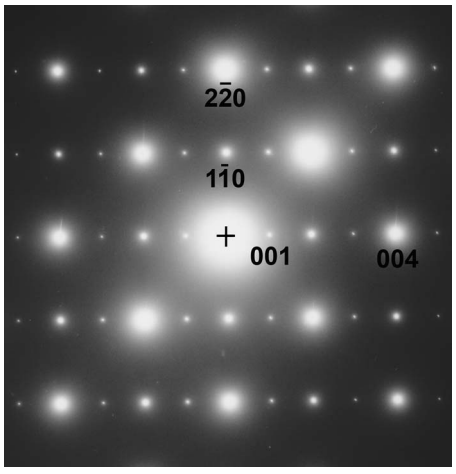

FIG. 4. Magnified and rotated part of the selected area diffraction pattern shown in Fig. 3. The indexing was made according to a simulation and a comparison with literature.

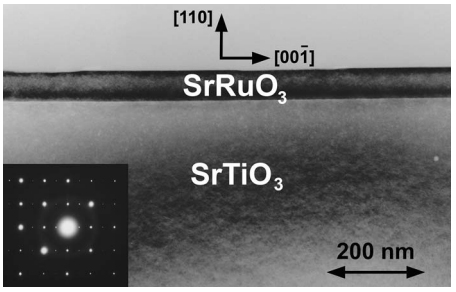

FIG. 5. Cross-section TEM image of the 60-nm-thick $SrRuO_3$ film. The crystallographic directions are indicated. The inset shows the corresponding diffraction pattern.

along the $(1\bar{1}0)_o$ plane, with the steps of the vicinal substrate running parallel to this plane. For the details of the crystallography of $SrRuO_3$ films growing on vicinal $SrTiO_3$ substrates, cf. Ref. 3.

From the TEM and SAED investigations it is concluded that the entire $SrRuO_3$ film has a uniform orientation, i.e., that no orientation domains of appreciable size and number are present. Such domains were found by other authors, e.g., in Refs. 22 and 23. Only in very few, exceptional cases, dark-field images of our film revealed a very small domain of an orientation differing from the main orientation. The volume share of such domains is negligible in our film.

Figure 6 shows a plan-view TEM image of the 5-nm-thin SRO film. No misfit dislocations are visible due to the fact that the film is coherently strained on the $SrTiO_3$ substrate. The pattern of lines running perpendicular to the $[1\bar{1}0]$ direction represent the step-terrace structure with an approximate step distance (terrace width) of 270 nm. The film is too thin, and bends too extensively under the electron beam, to obtain reliable TEM diffraction data.

B. Magnetization measurements

Figure 7 shows the magnetic moment of the 40-nm-thick SRO film as a function of temperature and magnetic field for various crystallographic directions as determined from the AFM and TEM studies. In all cases zero-field-cooled (ZFC, not shown), FC, and remanence (REM) sweeps were made. Whereas the ZFC magnetic moments were clearly smaller than the FC ones due to the large coercivity at low tempera-

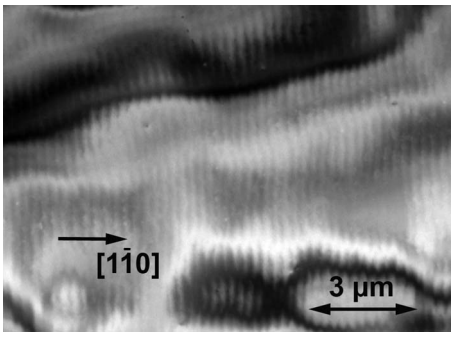

FIG. 6. Plan-view TEM image of the 5-nm-thick $SrRuO_3$ film with crystallographic directions indicated.

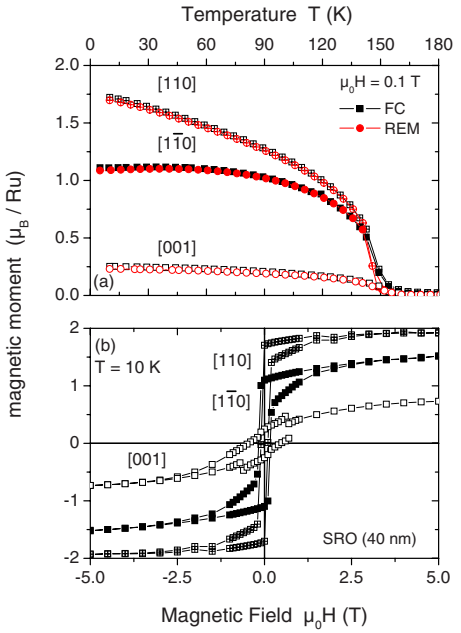

FIG. 7. (Color online) 40 nm $SrRuO_3$: (a) magnetic moment per Ru ion as a function of temperature. Measurements were done in FC and remanence (REM) mode. (b) Magnetic moment hysteresis curves at 10 K. The measurements were made with the magnetic field applied along the various crystallographic directions indicated in the figure. The kinks near ± 0.5 T for the [001] curve are measurement artifacts.

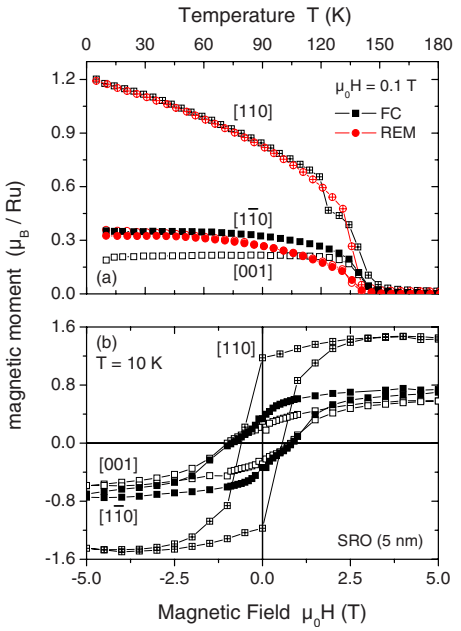

FIG. 8. (Color online) 5 nm $SrRuO_3$: (a) magnetic moment per Ru ion as a function of temperature. Measurements were done in FC and REM mode. (b) Magnetic moment hysteresis curves at 5 K. The measurements were made with the magnetic field applied along the various crystallographic directions indicated in the figure. Note that in (a) the remanent magnetic moment curves in the $[001]_o$ and $[1\bar{1}0]_o$ directions are nearly identical.

tures, the remanence is in all cases close to the FC magnetic moment, indicating square hysteresis loops. Indeed, hysteresis loops along the $[110]_o$ directions are rather square showing that the easy axis should be close to this direction, see Fig. 7(b). The diamagnetic contributions of the substrate and sample holder were determined from the high-field slope of the magnetic moment and were subtracted; this procedure was chosen, since it is impossible to determine the diamagnetic contribution independently with sufficient precision. Note, however, that this procedure neglects paramagnetic contributions from the film itself and leads to different values of the saturation magnetic moment along the various crystallographic directions. This is clearly unphysical, so very probably there are reversible paramagnetic contributions to the magnetic moment in the $[1\bar{1}0]_o$ and $[001]_o$ direction due to magnetization rotation processes. The saturation magnetic moment at 10 K is about $1.9\mu_B$/Ru, somewhat larger than the value found in a single crystal.[2] Comparing the saturation values along the various crystallographic directions yields a first indication of the size of the magnetocrystalline anisotropy energy: $[110]_o < [1\bar{1}0]_o < [001]_o$. Coercive fields at 10 K were 100 mT ($[110]_o$), 165 mT ($[1\bar{1}0]_o$), and 465 mT ($[001]_o$).

Figure 8 shows the corresponding data for the 5-nm-thick SRO film; the indexing is done on the basis of the AFM measurements, i.e., under the assumption that the $[001]_o$ direction is along the terraces of the $SrTiO_3$ substrate. Overall the appearance of the magnetic moment is similar to that of the thicker film but there are some significant differences. Whereas the $[110]_o$ direction is still close to the easy-axis direction, the in-plane anisotropy between $[1\bar{1}0]_o$ and $[001]_o$ is lost in the hysteresis and remanence curves. Note that the film behaves unconventional in the sense that along $[001]_o$ the remanent magnetic moment is higher than the FC one; at present we do not have any explanation for that. The saturation magnetic moment at 10 K is $1.5\mu_B$/Ru, considerably lower than for the 40-nm-thick film. This might be related to the higher coercivities that were much larger than for the thicker film with 567 mT ($[110]_o$), 856 mT ($[1\bar{1}0]_o$), and 900 mT ($[001]_o$). In view of the TEM result showing a dislocation network for the 60-nm-thick film, but coherent strain for the 5 nm thick film, one might conclude that the magnetization reversal process is controlled by nucleation of reverse domains and not by domain-wall motion. Since the thicker film has more nucleation centers at the dislocations, the coercive fields are lower. Main conclusion from these magnetization data is the presence of an easy axis close to the $[110]_o$ direction (parallel to the substrate normal) for both films and an almost isotropic magnetocrystalline anisotropy energy within the film plane for the 5-nm-thick film.

More detailed magnetization studies could only be made on the thicker SRO film since the SQUID magnetometer signal from the 5-nm-thick film was too small. Figure 9 shows angular sweeps of the magnetic moment recorded in an applied field of 3 T and various temperatures for rotations in the (a) $(001)_o$ and (b) $(1\bar{1}0)_o$ plane, respectively. θ_F denotes the angle between magnetic field and the surface normal ($[110]_o$). The data are not straightforward to interpret since the magnetic field might not be sufficient to force the magnetization vector into the respective crystallographic

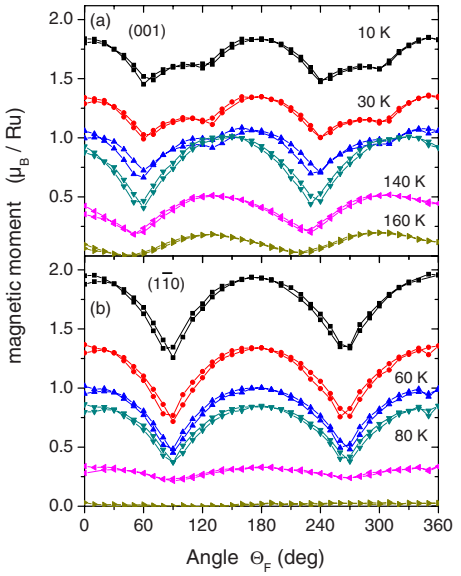

FIG. 9. (Color online) 40 nm $SrRuO_3$: angular sweeps at various temperatures with the magnetic field rotating in the (a) $(001)_o$ and (b) $(1\bar{1}0)_o$ plane. Before each sweep the film was demagnetized along the $[110]_o$ direction before applying the magnetic field of 3 T. The minima mark the location of magnetocrystalline energy maxima, the maxima the location of magnetocrystalline energy minima in the respective crystallographic planes.

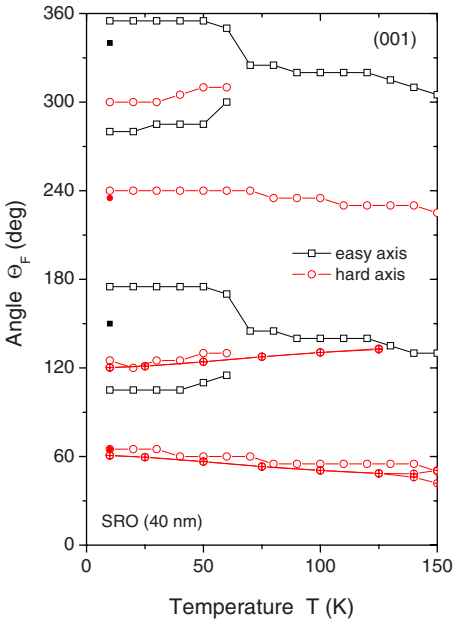

FIG. 10. (Color online) 40 nm $SrRuO_3$: magnetic hard- and easy-axes directions in the $(001)_o$ plane as determined from angular-dependent magnetization (open symbols) and magnetoresistance (crossed symbols) measurements. Solid symbols show the direction of the easy axes as determined from remanence measurements at 10 K.

planes. However, it is possible to arrive at some important conclusions by analyzing the symmetry of the curves. The magnetization rotation patterns in the $(1\bar{1}0)_o$ plane have twofold symmetry with maxima along $[110]_o$ and $[\bar{1}\bar{1}0]_o$ and minima along $[001]_o$ and $[00\bar{1}]_o$ directions. In view of the magnetization hysteresis curves in Fig. 7 the $[001]_o$ axis is therefore identified as hard axis; the easy axis should lie in the $(001)_o$ plane. The magnetization rotation patterns in the $(001)_o$ plane show a transition from a twofold symmetry above 70 K to a more complicated symmetry below 60 K. This might be interpreted as a transition in the magnetocrystalline energy with a turning of the easy axis. The location of the minima and maxima is temperature dependent[25] and is plotted in Fig. 10. Above 70 K the easy axis lies in the $(001)_o$ plane under an angle of about 35°, below 60 K there are two easy axes in the $(001)_o$ plane under angles of 5° and 75° from the $[110]_o$ direction. Earlier measurements did not detect the transition in the magnetocrystalline anisotropy.[5,6] This might be due to the fact that in those studies the remanent magnetization was investigated. In agreement with this, rotational sweeps of the remanent magnetization of our film only yield a twofold pattern in the $(001)_o$ plane at 10 K with an easy axis under an angle of about 30° with respect to $[110]_o$ as shown by the solid points in Fig. 10. This latter measurement leads to an easy-axis direction above 70 K approximately along $[310]_o$ in agreement with previous reports.[5,6]

The analysis of these measurements on the 40-nm-thick SRO film is in agreement with previous results:[5,6] the easy axis lies in the $(001)_o$ plane under an angle of about 35° with respect to the $[110]_o$ axis. This is also consistent with the TEM analysis that showed only a negligible fraction of 90° misaligned crystallographic domains. Beyond these results, a transition in the shape of the magnetocrystalline energy surface between 60 and 70 K was found. The data do not necessarily imply the presence of two easy-axis directions in the $(001)_o$ plane but probably local energy minima develop close to this plane.

C. Magnetotransport measurements

In this section the anisotropy of the SRO films is investigated using angular-dependent magnetoresistance measurements. This allows for a cross-check of the results of the 40-nm-thick film against the magnetization data, but, more importantly, yields a tool for the study of the anisotropy of much thinner films.

Figure 11 shows the zero-field resistivity of the (a) 40-nm-thick and (b) 5-nm-thick SRO film. The residual resistivity ratios for the 40-nm-thick film are 8.5 and 6.5 along the [001] and $[1\bar{1}0]$ directions, respectively; this compares well with the value of 6 found for an unstrained film by Gan *et al.*,[17] but is somewhat lower than the value of 11 reported by Klein *et al.*,[26] both for 100-nm-thick films. For the 5-nm-thick film the residual resistivity ratio is about 4 in agreement with the value reported by Schultz *et al.*[9] for a 6-nm-thick film. The ferromagnetic transition is clearly identified by the slope change in the curves.[26,27] In case of the 40-nm-thick film the resistivities along both principal in-plane directions were measured and were found to be distinctly different.[26] This already indicates that the transport properties are strongly dependent on crystallographic directions.

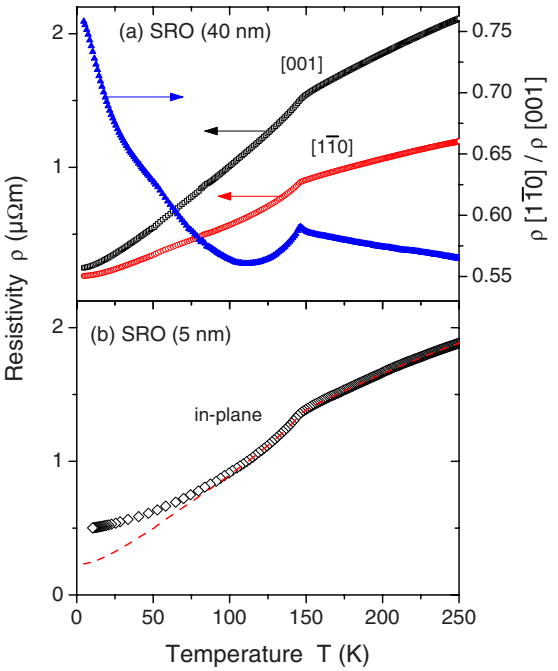

FIG. 11. (Color online) Resistivity of the (a) 40-nm-thick and (b) 5-nm-thick $SrRuO_3$ films. For the 40-nm-thick film, the resistivities along both principal in-plane directions were measured. The ratio of the corresponding resistivities is shown in (a) (right axis). The dashed line in (b) was obtained by averaging the resistivities in (a).

The ratio of the corresponding resistivities shows a clear anomaly at the Curie temperature. This must be due to magnetic domain-wall scattering since there are no reports of a structural change accompanying the paramagnetic-to-ferromagnetic transition. The data are consistent with published data[28,29] showing a preferential orientation of the magnetic domain walls along $[1\bar{1}0]_o$ and an enhanced zero-field resistivity for current densities along $[001]_o$. The resistivity of the 5-nm-thick film was only measured along one crystallographic direction. In the temperature range between 100 and 250 K it can be well reproduced by an average of 75% $\rho_{[001]}$ and 25% $\rho_{[1\bar{1}0]}$, see dashed line in Fig. 11(b). The deviations below 100 K might be due to a decrease in the mean-free path caused by microstructural disorder.[30,31]

In the following the magnetoresistance of the films is studied. Figure 12 shows magnetoresistance hysteresis curves of the 5-nm-thick $SrRuO_3$ film measured in a magnetic field parallel to $[1\bar{1}0]_o$. In the longitudinal configuration $(\vec{j}\|\vec{H})$ the magnetoresistance is negative with maxima and in the transverse configuration $(\vec{j}\perp\vec{H})$ the magnetoresistance is positive with minima at the coercive fields. This clear anisotropy shows that the main magnetoresistance contribution is from anisotropic magnetoresistance.[32,33]

Figure 13 shows angular magnetoresistance hysteresis curves at 150 K in an applied field of $\mu_0 H = 8$ T. The four panels correspond to magnetic field rotations in the [(a) and (b)] $(001)_o$ and [(c) and (d)] $(1\bar{1}0)_o$ planes with both longitudinal and transverse configuration shown. According to the analysis in the theory section, under the assumption that the

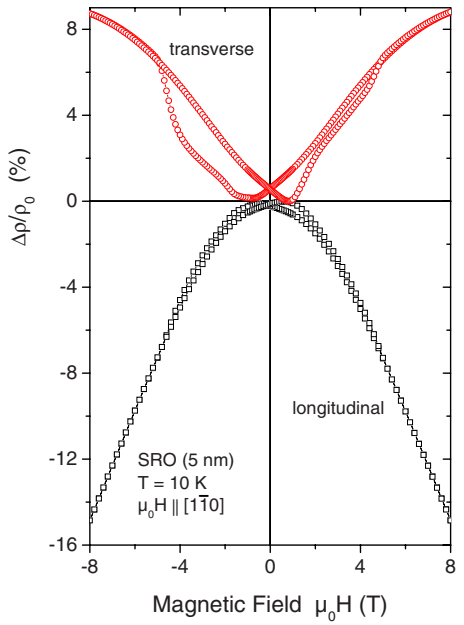

FIG. 12. (Color online) Magnetoresistance hysteresis curves of the 5-nm-thick $SrRuO_3$ film at 10 K in an in-plane magnetic field. The magnetic field was applied in longitudinal $(\vec{j}\|\vec{H})$ and transverse $(\vec{j}\perp\vec{H})$ direction.

magnetization vector follows the magnetic field vector, the angular-dependent curves can be described by an expansion in $\cos(2n\theta)$ and $\sin(2n\theta)$ with the coefficients determined by the crystalline symmetry. Accordingly, the solid red lines are fits of the expressions for orthorhombic symmetry up to eighth order to the data as given in Eqs. (6)–(9). For rotations in the $(1\bar{1}0)_o$ plane, (c) and (d), the agreement is very good

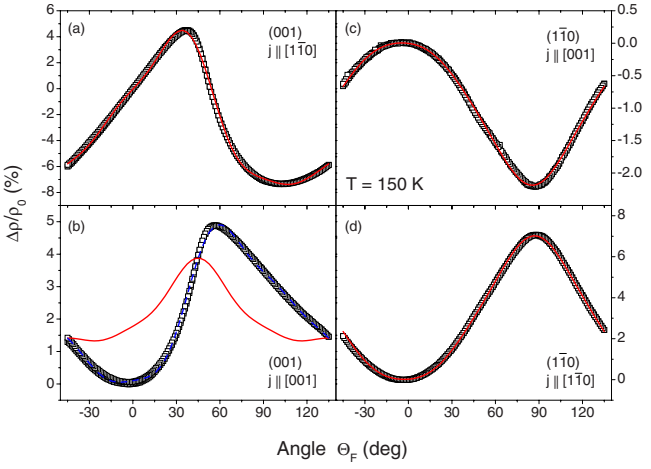

FIG. 13. (Color online) 40 nm $SrRuO_3$: angular hysteresis curves of the magnetoresistance at 150 K in an applied field of $\mu_0 H = 8$ T. In (a) and (b), the field was rotated within the $(001)_o$ plane with the current density flowing along (a) $[1\bar{1}0]_o$ and (b) $[001]_o$. In (c) and (d), the field was rotated within the $(1\bar{1}0)_o$ plane with the current density flowing along (a) $[001]_o$ and (b) $[1\bar{1}0]_o$. The solid red lines are fits of the expressions for orthorhombic symmetry to the data as explained in the text. The dashed blue line in (b) is a fit of the expression for monoclinic symmetry to the data.

and the data basically follow a $\cos(2\theta)$ dependence. This is consistent with the corresponding magnetization rotation data in Fig. 9. For rotations in the $(001)_o$ plane no evident symmetry is observed with respect to the $[110]_o$ and $[1\bar{1}0]_o$ directions, indicating, in agreement with the magnetization results, that the easy and hard axes are not aligned with directions of highest symmetry. Whereas the longitudinal magnetoresistance can be satisfactorily fitted by Eq. (6), the transverse magnetoresistance curves in Fig. 13(b) do not agree at all. This indicates that the sample does actually not have orthorhombic but lower symmetry. The dashed blue line in Fig. 13(b) is a fit of Eq. (13) for monoclinic symmetry to the data. Here the agreement is very good; this shows that the angle between the $[100]_o$ and $[010]_o$ directions slightly deviates from 90°. Moreover, the magnetoresistance data are consistent with a right angle between the $[110]_o$ and the $[001]_o$ directions; thus there is no indication of a triclinic deformation.

The failure of the expression for orthorhombic symmetry to fit the data in Fig. 13(b) is not due to the truncation of the series since higher-order terms just yield rapid oscillations that are not observed experimentally. The main effect of the monoclinic symmetry is to generate a $\cos(2\theta)$ term that is absent in the series expansion for orthorhombic symmetry but is observed experimentally. The coefficient of this $\cos(2\theta)$ term vanishes when the angular deviation from 90° vanishes. Since this deviation is on the order of 1° in the $SrRuO_3$ films,[3] one might *a priori* expect this coefficient to be small. However, experimentally it is impossible to vary this angle in the $SrRuO_3$ films continuously, so no data are available on the size of the coefficient and its behavior as a function of angular deviation. The data presented here indicate that the effect of a small angular deviation on the magnetoresistance is significant and might be used as a fingerprint for the symmetry.

Figure 14 shows equivalent angular magnetoresistance hysteresis curves recorded at 10 K. Whereas the overall symmetry of the curves does not change on cooling from 150 to 10 K, sharp jumps appear for rotations in the $(001)_o$ and cusps for rotations in the $(1\bar{1}0)_o$ plane. These jumps and cusps are due to the strong magnetocrystalline anisotropy that leads to a sudden angular jump of the magnetization vector when the applied magnetic field sweeps across a magnetic hard axis. Accordingly, the angular position of the jumps and cusps marks the location of the hard axes. For the $(001)_o$ rotational sweep the direction of the hard axis was determined from magnetoresistance measurements at various temperatures and is plotted in Fig. 10. Good agreement with the magnetization results was found.

Fitting of the magnetoresistance curves was done iteratively using Eqs. (12)–(15) for the magnetoresistance and Eq. (16) for the magnetocrystalline anisotropy in monoclinic symmetry up to fourth order. First, the angular dependence of the anisotropy energies was constructed from the location of the hard-axis and easy-axis directions as shown in Fig. 10. In general the angle θ between the magnetization and the surface normal does not agree with the angle θ_F between the magnetic field and the surface normal. θ was determined from θ_F within a domain rotation model by minimizing the

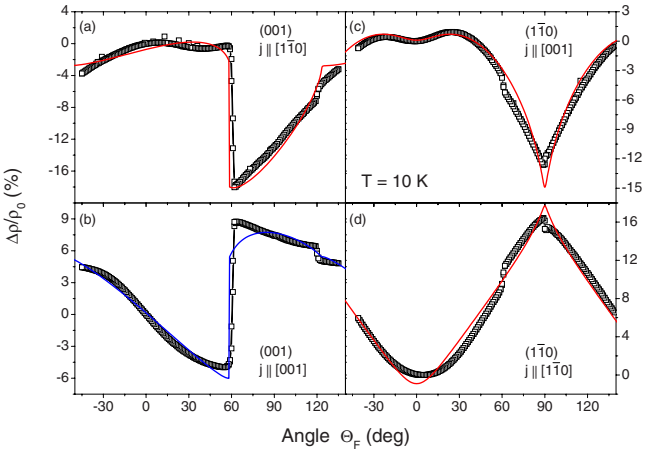

FIG. 14. (Color online) 40 nm $SrRuO_3$: angular hysteresis curves of the magnetoresistance at 10 K in an applied field of $\mu_0 H = 8$ T. In (a) and (b), the field was rotated within the $(001)_o$ plane with the current density flowing along (a) $[1\bar{1}0]_o$ and (b) $[001]_o$. In (c) and (d), the field was rotated within the $(1\bar{1}0)_o$ plane with the current density flowing along (a) $[001]_o$ and (b) $[1\bar{1}0]_o$. The solid lines were obtained by an iterative procedure using both the expressions for the magnetoresistance and magnetocrystalline anisotropy energy in monoclinic symmetry.

total energy $E_Z + E_K = \mu_0 \vec{M}_S \cdot \vec{H} + E_K$. Then the sets of parameters $(s_{2n}, c_{2n}, n \leq 2)$ of the magnetoresistance and $(K_{s2n}, K_{c2n}, n \leq 2)$ of the magnetocrystalline energy were iteratively varied. The magnetoresistance fits are shown in Fig. 14. The variation in the corresponding cross sections through the magnetocrystalline energy landscape in the $(001)_o$ and $(1\bar{1}0)_o$ planes is shown in Fig. 15. Compared to LSMO that has a cubic magnetocrystalline anisotropy constant $K_1 \simeq -3$ kJ/m^3 at 10 K the magnetocrystalline anisotropy of the $SrRuO_3$ film is very large. In the hard directions the anisotropy field can reach $2K/M_S \simeq 5$ T($\mu_0 M_S = 0.25$ T).

This analysis of the 10 K data corroborates the conclusion obtained from the 150 K data of the presence of monoclinic

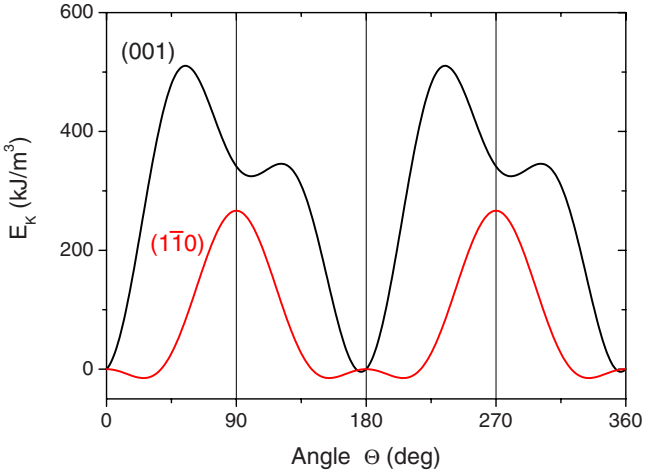

FIG. 15. (Color online) Cross-sectional cuts through the magnetocrystalline anisotropy energy surface at 10 K in the $(001)_o$ and $(1\bar{1}0)_o$ planes. These data were constructed from the fits to the magnetoresistance data in Fig. 14.

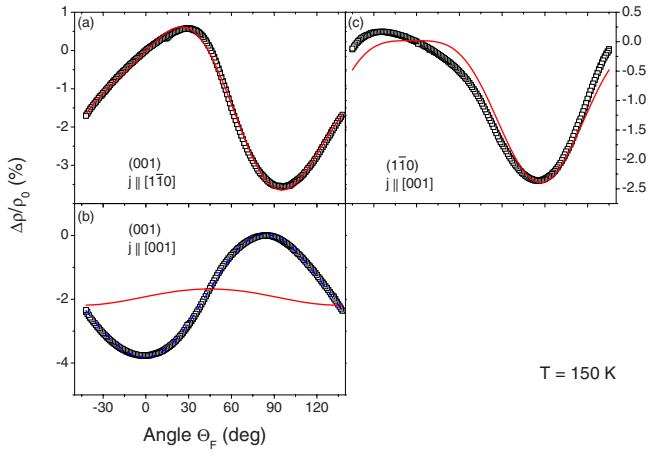

FIG. 16. (Color online) 5 nm $SrRuO_3/SrTiO_3$: angular hysteresis curves of the magnetoresistance at 150 K in an applied field of $\mu_0 H=8$ T. In (a) and (b), the field was rotated within the $(001)_o$ plane with the current density flowing along (a) $[1\bar{1}0]_o$ and (b) $[001]_o$. In (c), the field was rotated within the $(1\bar{1}0)_o$ plane with the current density flowing along $[001]_o$. The solid red lines are fits of the expressions for orthorhombic symmetry to the data according to Eqs. (6)–(8). The dashed blue line in (b) is a fit of the corresponding expression for monoclinic symmetry, Eq. (13).

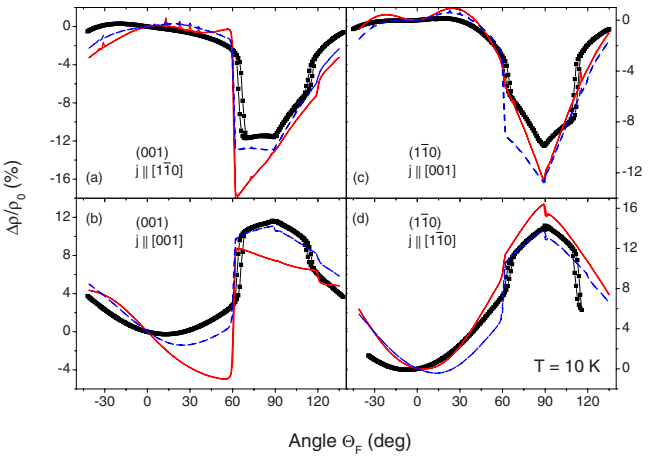

FIG. 17. (Color online) 5 nm $SrRuO_3$: angular hysteresis curves of the magnetoresistance at 10 K in an applied field of $\mu_0 H=8$ T. In (a) and (b), the field was rotated within the $(001)_o$ plane with the current density flowing along (a) $[1\bar{1}0]_o$ and (b) $[001]_o$. In (c) and (d), the field was rotated within the $(1\bar{1}0)_o$ plane with the current density flowing along (a) $[001]_o$ and (b) $[1\bar{1}0]_o$. The solid red lines are the magnetoresistance of the 40-nm-thick $SrRuO_3$ film, the dashed blue lines are an average magnetoresistance as explained in the text.

symmetry. Moreover, the magnetocrystalline anisotropy constants could be determined from the variation in the magnetization angle as a function of the magnetic field angle.

Whereas measurements and analysis of the 40-nm-thick film mainly served to establish a reference system, important insights are expected from the magnetoresistance measurements on the 5-nm-thick film, since in this case SQUID magnetometry did not yield any results due to the small signal. Figure 16 shows the longitudinal and transverse magnetoresistance at 150 K for rotations in the $(001)_o$ and $(1\bar{1}0)_o$ plane. Whereas the overall symmetry is similar to that in Fig. 13, there are small, but significant deviations in the magnetoresistance curves from the expected symmetry. The most stringent test is provided by the angular variation in the magnetoresistance in the $(1\bar{1}0)_o$ plane, since this, according to Eq. (14), is characterized by only three expansion coefficients as opposed to five coefficients allowed for rotations in the $(001)_o$ plane, see Eqs. (12) and (13). Indeed, the fitting does not reproduce the data too well, see Fig. 16(c). This indicates that the 5-nm-thick $SrRuO_3$ film does not have a uniform orientation of the crystallographic domains. This is corroborated by the 10 K magnetoresistance data presented in Fig. 17. The symbols represent the data for the 5-nm-thick film; the solid red lines, the corresponding data from the 40-nm-thick sample from Fig. 14. From a qualitative comparison it is seen that the measured curves of the 5 nm $SrRuO_3$ film in all configurations show magnetoresistance characteristics of both crystallographic domains: as an example in Fig. 17(a) the magnetoresistance for rotations in the $(001)_o$ plane with current density along $[1\bar{1}0]_o$ shows the sharp jump near 65° as is characteristic for the $[001]_o$ crystallographic domains but does also show the cusp near 90° characteristic of the $[1\bar{1}0]_o$ domains. The dashed blue lines were obtained by adding a fraction p of the magnetoresistance of the misaligned domains to the fraction $(1-p)$ of the magnetoresistance of the orderly aligned domains. This does not lead to perfect agreement with the measured data but shows the similarity of the characteristic features in both data and calculated curves. This comparison indicates that there is a fraction of about 30–40 % of crystallographic domains with their $[001]_o$ axes not aligned with the terrace edge direction of the substrate. A fit of Eqs. (12)–(15) in conjunction with Eq. (16) to the data was not attempted since the number of fitting parameters was too large.

V. SUMMARY AND CONCLUSIONS

In this work the structural, magnetic and magnetotransport properties of three $SrRuO_3$ films with respective thicknesses of 5, 40, and 60 nm grown on $SrTiO_3$ (001) were investigated. Transmission electron microscopy showed that the 60-nm-thick film had long-range crystallographic order with the $[110]_o$ direction along the surface normal and the $[001]_o$ axis along the terraces of a vicinal substrate with small miscut angle, which in turn are along the [100] direction of the $SrTiO_3$ (001) substrate. Magnetization and magnetoresistance measurements lead to the same conclusion for the 40-nm-thick film. These results are in agreement with previous reports.[5,6] Above 70 K the easy-axis direction was found to be in the $(001)_o$ plane under about 35° with respect to the substrate normal, below 60 K the presence of two magnetization maxima indicates easy-axes directions in the $(001)_o$ plane under 5° and 75° with respect to the substrate normal. This 40-nm-thick film was used as a reference system to determine the symmetry of the angular-dependent magnetoresistance. Analysis of this showed a monoclinic

distortion of the $SrRuO_3$ crystal lattice within the $(001)_o$ plane. These magnetoresistance data were used as a fingerprint in the analysis of the magnetoresistance of the 5-nm-thick film. Although for this film the orientation of the crystallographic domains could not be determined from transmission electron microscopy and the magnetocrystalline anisotropy could not be studied by angular-dependent SQUID magnetometry, magnetoresistance measurements could be readily made. The symmetry of the angular magnetoresistance showed that the thin $SrRuO_3$ film did not have a uniform crystallographic orientation, but had about 30–40 % of the crystallographic domains misaligned with the $[001]_o$ axis perpendicular to the terraces of the vicinal substrate. This is a surprising result, since both the 5- and the 40-nm-thin films were deposited in the step-flow growth regime. The crystallographic properties of thin $SrRuO_3$ films play a vital role in heterostructures and will have a significant impact on the magnetic and magnetotransport properties of, e.g., exchange-coupled $La_{0.7}Sr_{0.3}MnO_3/SrRuO_3$ superlattices.[10]

ACKNOWLEDGMENTS

This work was supported by the German Science Foundation (DFG) within the Collaborative Research Center SFB 762 "Functionality of Oxide Interfaces."

*ziese@physik.uni-leipzig.de
†vrejoiu@mpi-halle.de

[1] C. W. Jones, P. D. Battle, P. Lightfood, and W. T. A. Harrison, Acta Crystallogr., Sect. C: Cryst. Struct. Commun. **45**, 365 (1989).
[2] G. Cao, S. McCall, M. Shepard, J. E. Crow, and R. P. Guertin, Phys. Rev. B **56**, 321 (1997).
[3] Q. Gan, R. A. Rao, C. B. Eom, L. Wu, and F. Tsui, J. Appl. Phys. **85**, 5297 (1999).
[4] G. Herranz, F. Sánchez, J. Fontcuberta, M. V. García-Cuenca, C. Ferrater, M. Varela, T. Angelova, A. Cros, and A. Cantarero, Phys. Rev. B **71**, 174411 (2005).
[5] S. Kolesnik, Y. Z. Yoo, O. Chmaissem, B. Dabrowski, T. Maxwell, C. W. Kimball, and A. P. Genis, J. Appl. Phys. **99**, 08F501 (2006).
[6] Y. Z. Yoo, O. Chmaissem, S. Kolesnik, A. Ullah, L. B. Lurio, D. E. Brown, J. Brady, B. Dabrowski, C. W. Kimball, M. Haji-Sheikh, and A. P. Genis, Appl. Phys. Lett. **89**, 124104 (2006).
[7] B. W. Lee, C. U. Jung, M. Kawasaki, and Y. Tokura, J. Appl. Phys. **104**, 103909 (2008).
[8] A. Vailionis, W. Siemons, and G. Koster, Appl. Phys. Lett. **93**, 051909 (2008).
[9] M. Schultz, S. Levy, J. W. Reiner, and L. Klein, Phys. Rev. B **79**, 125444 (2009).
[10] M. Ziese, I. Vrejoiu, E. Pippel, P. Esquinazi, D. Hesse, C. Etz, J. Henk, A. Ernst, I. V. Maznichenko, W. Hergert, and I. Mertig, Phys. Rev. Lett. **104**, 167203 (2010).
[11] R. R. Birss, *Symmetry and Magnetism* (North-Holland, Amsterdam, 1964).
[12] P. K. Muduli, K.-J. Friedland, J. Herfort, H.-P. Schönherr, and K. H. Ploog, Phys. Rev. B **72**, 104430 (2005).
[13] W. Limmer, J. Daeubler, L. Dreher, M. Glunk, W. Schoch, S. Schwaiger, and R. Sauer, Phys. Rev. B **77**, 205210 (2008).
[14] W. Döring, Ann. Phys. **456**, 102 (1957).
[15] W. Döring and G. Simon, Ann. Phys. **460**, 373 (1960).
[16] W. Döring and G. Simon, Ann. Phys. **463**, 144 (1961).
[17] Q. Gan, R. A. Rao, C. B. Eom, J. L. Garrett, and M. Lee, Appl. Phys. Lett. **72**, 978 (1998).
[18] X. Q. Pan, J. C. Jiang, W. Tian, Q. Gan, R. A. Rao, and C. B. Eom, J. Appl. Phys. **86**, 4188 (1999).
[19] K. Takahashi, T. Oikawa, K. Saito, S. Kaneko, H. Fujisawa, M. Shimizu, and H. Funakubo, Jpn. J. Appl. Phys., Part 1 **41**, 5376 (2002).
[20] I. Vrejoiu, G. Le Rhun, L. Pintilie, D. Hesse, M. Alexe, and U. Gösele, Adv. Mater. **18**, 1657 (2006).
[21] M. Ziese, I. Vrejoiu, A. Setzer, A. Lotnyk, and D. Hesse, New J. Phys. **10**, 063024 (2008).
[22] J. C. Jiang, W. Tian, X. Pan, Q. Gan, and C. Eom, Appl. Phys. Lett. **72**, 2963 (1998).
[23] J. C. Jiang, W. Tian, X. Pan, Q. Gan, and C. Eom, Mater. Sci. Eng., B **56**, 152 (1998).
[24] S. H. Oh and C. G. Park, J. Appl. Phys. **95**, 4691 (2004).
[25] L. Klein, J. S. Dodge, C. H. Ahn, J. W. Reiner, L. Mieville, T. H. Geballe, M. R. Beasley, and A. Kapitulnik, J. Phys.: Condens. Matter **8**, 10111 (1996).
[26] L. Klein, J. S. Dodge, C. H. Ahn, G. J. Snyder, T. H. Geballe, M. R. Beasley, and A. Kapitulnik, Phys. Rev. Lett. **77**, 2774 (1996).
[27] Y. Kats, L. Klein, J. W. Reiner, T. H. Geballe, M. R. Beasley, and A. Kapitulnik, Phys. Rev. B **63**, 054435 (2001).
[28] A. F. Marshall, L. Klein, J. S. Dodge, C. H. Ahn, J. W. Reiner, L. Mieville, L. Antagonazza, A. Kapitulnik, T. H. Geballe, and M. R. Beasley, J. Appl. Phys. **85**, 4131 (1999).
[29] L. Klein, Y. Kats, A. F. Marshall, J. W. Reiner, T. H. Geballe, M. R. Beasley, and A. Kapitulnik, Phys. Rev. Lett. **84**, 6090 (2000).
[30] G. Herranz, B. Martínez, J. Fontcuberta, F. Sánchez, C. Ferrater, M. V. García-Cuenca, and M. Varela, Phys. Rev. B **67**, 174423 (2003).
[31] G. Herranz, V. Laukhin, F. Sánchez, P. Levy, C. Ferrater, M. V. García-Cuenca, M. Varela, and J. Fontcuberta, Phys. Rev. B **77**, 165114 (2008).
[32] D. B. Kacedon, R. A. Rao, and C. B. Eom, Appl. Phys. Lett. **71**, 1724 (1997).
[33] R. A. Rao, D. B. Kacedon, and C. B. Eom, J. Appl. Phys. **83**, 6995 (1998).